S1. X-ray reflectivity theoretical background

The X-ray reflectivity (XRR) technique was initially developed in 1954 by L. G. Parratt to explore the surface of copper-coated glasses. [1] Since then, XRR becomes a well-established structural characterization technique to study a wide variety of materials important in several research fields, e.g, Physics, Chemistry, Biology, Materials Science, etc. [1-5] In the X-ray reflectivity measurements, the X-rays are reflected from an interface such as the sample's surface and the reflected intensity scattered in the specular direction is registered. If the interface is perfectly sharp, then the reflected intensity follows the law of Fresnel reflectivity. Otherwise, it will deviate from the predictions. The deviations may be analytically accounted for to obtain the density profile of the interfaces normal to the surface, thickness and roughness. Through the simulations of the measured curves using Parratt's recursive formalism employing the dynamical theory of X-ray scattering, [2,6] the refractive indexes of the individual layers of the stacked structure, n_j, are estimated. n_j is given by:

$$n_j = 1 - \delta_j - i\beta_j \qquad \text{Eq. S1.1}$$

where the critical angle is proportional to δ, $\sqrt{2\delta}$. δ, is, in turn, proportional to the density of the material, ρ, through

$$\delta_j = \frac{10^6 \nu \rho_j \sum_j x_j (Z_j + f_j')}{\sum_j (M_j)} \; ; \; \beta_j = \sum_{j=1}^{N} \frac{\nu \rho_j (f_j'')}{M_j} 10^6 \qquad \text{Eq. S1.2}$$

where the summation is performed over all the atoms present in the compound. $\nu = \frac{Na \, r_e \lambda^2}{2\pi}$, r_e is the classical electron radius (2.818×10^{-5} Å), Na is the Avogadro number, x_j is the atomic ratio of atom j, Z_j is the atomic number of atom j and f_j' is the real part anomalous dispersion term of the atomic scattering factors for a given atom j. On the other hand, the scattering length density (SLD) may be defined as:

$$SLD \equiv \zeta = \frac{2\pi(\delta + i\beta)}{\lambda^2} \qquad \text{Eq. S1.3}$$

where λ is the X-ray wavelength (1.54056 Å for Cu Kα_1).

Follows the procedure to determine the reflectivity at the surface of a generic layered structure. Figure S1.1 shows a multilayer structure that may be considered as a stratified medium on top of an infinitely thick substrate. t represents the thickness of the individual layers down to N (index # of the substrate). Each layer is also defined by a homogenous mass density along its thickness and a refractive index calculated according to Eq. S1.1. By definition, the incident angle (θ_i) equals the reflected one (θ_r) in specular X-ray reflectivity measurements. Thus, due to geometrical

considerations, Q_z is perpendicular to the sample as represented in figure S1.1. Because of the in-plane continuity condition, the in-plane projections of the incident and reflected wave-vectors are equal. Thus, $\vec{K_z}$ of the individual layers may be deduced:

$$K_{z,j} = \sqrt{(K_{z,0})^2 - 4\pi\zeta_j}$$

Eq. S1.4

And the same for the air/first interface:

$$K_{z,air} = \sqrt{\frac{(Q_z)^2}{4} + 4\pi\zeta_{air}}$$

Eq. S1.5

where $|\vec{Q_z}| = \frac{4\pi\,sin(\theta)}{\lambda}$ and $\zeta_{air}=1$ with a null complex component.
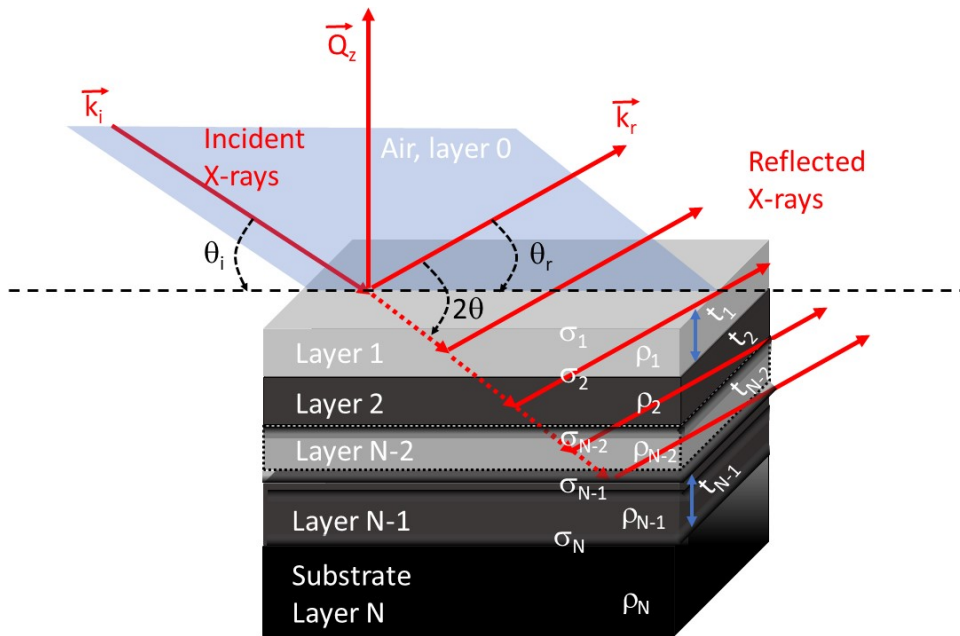

Figure S1.1 Schematic view of multilayer structure showing 4 layers on top of a substrate. Each layer is defined by a set of 3 independent quantities: thickness (t), density (ρ) and roughness (σ).

The reflectivity from the interface between layer j and j+1 is given by:

$$r_j = \frac{K_{z,j} - K_{z,j+1}}{K_{z,j} + K_{z,j+1}}exp\left(-2(\sigma_{j+1})^2 K_{z,j} - K_{z,j}K_{z,j+1}\right)$$

Eq. S1.6

where σ_{j+1} is the roughness of the j+1th layer. The decaying exponent term defines how much of the reflected beam is deviated from the specular condition, which according to the Fresnel law may be defined using the wavevectors for consecutive layers, i.e., $\dfrac{K_{z,j} - K_{z,j+1}}{K_{z,j} + K_{z,j+1}}$. Few words are required to justify the choice of the decaying in the reflectivity due to the presence of roughness. Depending on the Fourier components of the wavelength range, two possible types of roughness are to be distinguished: macroscopic roughness and microscopic or atomic roughness. The former is applied if the roughness period is large compared to the coherence length. Otherwise, the latter is applied. Moreover, the former is usually due to facets wider than the coherence length and with multi-angle orientation with respect to the X-ray beam. Macroscopic roughness has its finger print in a broader specular reflection than the resolution function of the diffractometer, i.e., when the resolution is determined by the angular width of the direct beam or when split peaks characterize the incident radiation. Therefore, since the incident angles are not well defined, a quantitative description of the macroscopic roughness is problematic and the used optics (slits, Göbel mirrors, monochromators, etc) approaches the issue as a slope error. Microscopic roughness, on the other hand, occurs on a much smaller scale than the coherence length. Therefore, it describes the distortions of the incident X-rays yielding a reduction of the intensity of the scattered beam as compared to an ideal interface. According to figure S1.1, the lateral component of $\vec{Q} = \vec{K}_r - \vec{K}_i$ is null and only the laterally averaged roughness is accounted for. In fact, the influence of point defects, islands, lateral steps, etc, may be neglected because of the non-dependence of $\vec{Q}$ with the surface plane. An assumption often used in the simulation of XRR scans is that the function that characterizes the height of the interface follows a Gaussian distribution. Therefore, it follows a laterally averaged density with the shape of the error function. Two common mathematical descriptions of the roughness are used in computer codes. The first, usually attributed to Lord Rayleigh is the mathematical treatment of the reflection of acoustic waves where the ideal reflectivity is multiplied by an exponential damping factor, $exp(-\sigma^2 |\vec{Q}|^2)$. The drawbacks of using the Rayleigh's mathematical treatment are the impossibility to use it in a multilayer system because it assumes the same roughness for all the layers and the wrong characterization of the angular regions in the vicinity of the critical angle. The second description has been proposed by Nevot and Crocé [8] and mathematically analyzed by Vidal and Vincent. [9] The model compares well to a discrete one since it is applied to each interface. This is the approach used in the MROX software. The reflected amplitude wave is analytically defined as

$$R_j = \frac{r_j + R_{j+1}\phi_j}{1 + r_j R_{j+1}\phi_j} \qquad\qquad \text{Eq. S1.7,}$$

Where ϕ_j is the phase of the reflected wave that depends on the thickness of layer j (t_j) according to $\phi_j = exp(2iK_{z,j+1} t_{j+1})$, and $r_{j,j+1}$ is calculated using Eq. S1.6 for layers j and j+1. Starting from the N-1 layer, Eq. S1.6 is calculated for r_{N-1} using $K_{z,N-1}$, $K_{z,N}$, σ_N, i.e., z-component of the wavevector and the roughness between the N-1 and the substrate interfaces, respectively. Then R_{N-1} includes the bottom reflectivity scattered by the substrate considered infinitely thick, i.e., $R_N = 0$, and Eq. S1.7 is reduced to $R_{N-1} = r_{N-1}$. Follows, the calculation of R_{N-2} which depends on r_{N-2}, $R_{N-1} = r_{N-1}$ and ϕ_{N-2}, a function of t_{N-1}, as well as $K_{z,N-2}$, $K_{z,N-1}$, and σ_{N-1}. Therefore, for the second iteration, the thickness density and roughness triplet are indexed to the first layer (with finite thickness) on top of the substrate. The calculation is executed recursively up to the

surface layer (pseudo-layer index # zero). The total reflectivity is calculated as $R = |R_0|^2$. The modulus of the reflectivity is required because $K_{z,j}$ and ϕ_j are complex numbers. The former due to the complex representation of the refractive index (or the SLD) while the latter corresponds to the phase of the reflected wave at each interface.

For the special case of quantum heterostructures such as the superlattices, according to the kinematical theory of the grazing incidence X-ray scattering, the angular separation between consecutive Kiessig fringes is size-effect dependent through an equivalent of Bragg's law,

$$t = \frac{n \cdot \lambda}{2 \cdot \left(sin\left(\frac{2\theta_j}{2}\right) - sin\left(\frac{2\theta_i}{2}\right) \right)}$$

. n is the diffraction order and the indices j and i are related to consecutive maxima/minima intensities defined by n and t is the layer thickness. The effect of adding extra layers further complicates the XRR pattern due to the multiple interference between individual planes of atoms in a given layer with the ones from the added layer. In the case of superlattice quantum heterostructures, the interference caused by the periodic structure continuously adds up as the number of periods increases. Such complex multiple interference phenomena are revealed in a XRR scan by the so-called superlattice diffraction orders (SL). The period of these oscillations can be used to infer layer thicknesses, interlayer roughness's, electron densities and their contrasts, and complex refractive indices (which depend on atomic number and atomic form factor), for example using the Abeles matrix formalism or the recursive Parratt-formalism as follows. The X-ray beam polarization plays a negligible effect. In fact, for σ-polarized X-ray radiation, C=1, while for π-polarized X-ray radiation, the grazing incidence angles in a XRR scan yields C=cos(2θ)→1. Assuming a negligible wavelength divergence ($\frac{\Delta\lambda}{\lambda} \to 0$) the thickness resolution (Δt) is mainly constrained to the angular resolution of the diffractometer equipment through $\frac{\partial t}{\partial \frac{2\theta}{2}} \Delta\left(\frac{2\theta}{2}\right)$. Thicknesses resolutions in the order of 0.1 Å or below are, consequently, derived when the angular separation between two consecutive KF is 0.001 ° in θ and the goniometer resolution for the same axis is one order of magnitude lower. Therefore, in a conventional diffractometer, the observation of thin layers is usually overcome by employing conventional optics and the limitation to the use of XRR arises for thicknesses in the order of several hundreds of Å. The limitation is explained by the decrease of the angular separation between consecutive KF with increasing thickness. As an example, a thick layer of 5000 Å is identifiable in a XRR scan through an angular separation of ~0.008° between two maxima/minima observed for consecutive KF or ~0.004 ° between the maximum and the following minimum. If 10 datapoints are measured in-between the range then a minimum step of <0.0004 ° is required (in θ) which is inaccessible to some conventional goniometers. Thinner layers are also well simulated by employing the kinematical theory of X-ray scattering while thicker layers require the use of the more advanced dynamical theory. Refraction effects and multiple scattering are highly relevant in thicker layers and not accounted in the former scattering theory. Therefore, a precision of at least 0.1 Å for the calculated thickness of the individual layers is accomplished by using the 220 Ge monochromator and the Soller slit employed in the measurements.

S2. MROX – the Multiple Reflection Optimization package for X-ray reflectivity software

MROX is developed using the MATLAB Graphical User Interface Development Environment (GUIDE) and intensively tested on MATLAB 2010b, 2011a, 2015a, 2020a, 2021b and 2022b. It is expected that this package to perform equally well in all other versions. The main areas (systems) of MROX principal functionalities may be summarized as depicted in figure S2.1. The seven main areas are: the systems concerning the license, the log, function hierarchy, layer operations, simulation, fitting and saving simulation or fit. A brief description of each block follows. A complete instructions manual may be also found on the MROX official website (www.MROX.eu).
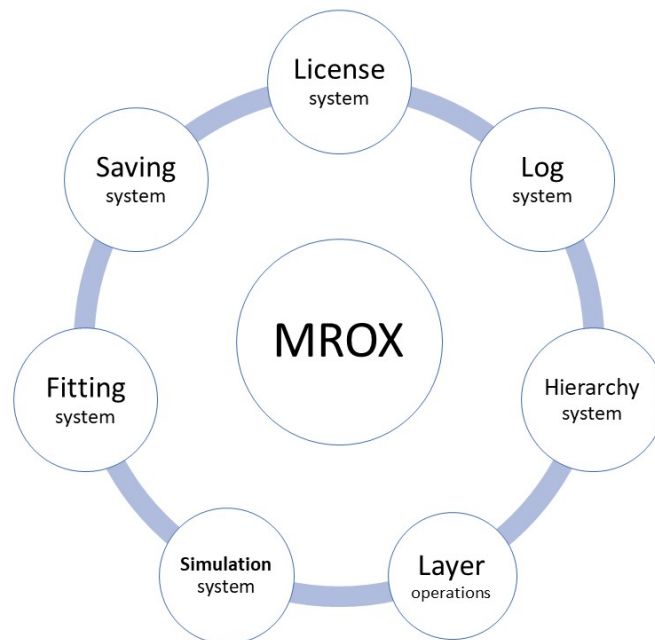

Figure S2.1 The seven main blocks where the MROX functionalities are developed and implemented.

License system MROX is free to use but the code is protected by the pcode MATLAB function. pcode generates content-obscured, executable files. If double-clicked, the pcode files are not readable by the interpreter. The main reason to encode the files is related to copyright issues where researchers may use the software without the appropriate citation which is unfair to the authors. Software development is highly time-consuming. MROX is deployed as two packages of licenses: demonstration and standard. In order to run MROX requires java installed in the destination machine. The 'standard' license contains a set of integers and chars and is sent to the user via email upon request. MROX uses a coded 2-step validation license procedure. If the license is invalid, MROX closes itself within the subsequent 5 seconds. The demonstration license, 'L000',

should be included in the license.dat file of the main MROX folder. With the demonstration license, the user is not capable of using the MROX outputs but all functionalities are available. Figure S2.2 highlights the MROX layout with a successful validation of the license.
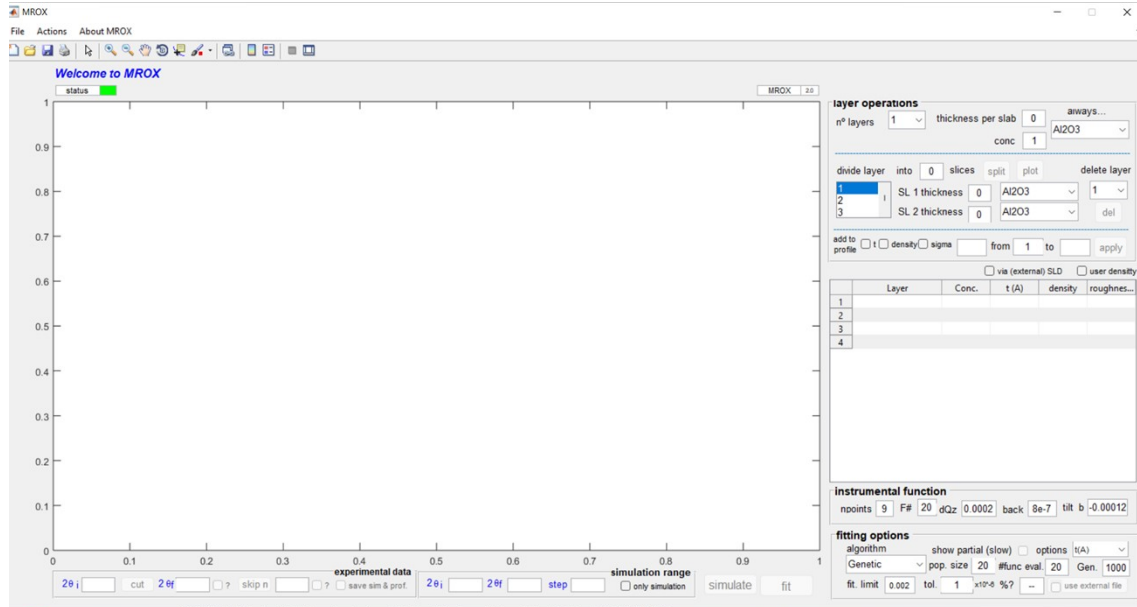

Figure S2.2 MROX layout (XRR version) highlighting a valid license (status is green). If the license is invalid, adminer.dat is not present (or is damaged or incorrect) in the current MROX folder or the license key is not or is expired then the status color is red.

The MROX interface consists of three main sections: the data and simulation/fitting visualization are conveyed to the central area, the selection of data range and skipping data points are located below the plotting section and functionalities related to the creation/edit/delete a layer structure as well as the instrumental/resolution function and the fitting options are operated on the right side of the user interface.

Log system Available in the main software folder, the *log.dat* is a register file of most activities of user interaction with MROX. It starts with a welcome message after license validation each time user runs MROX. All messages are saved in the *log.dat* file and are self-explanatory. The log system is intuitive and has the goal to help the user to track his/her actions with MROX.

Hierarchy system Developed using machine learning techniques, the hierarchy system prevents the user to perform operations, i.e., acting on MROX, that in a given moment of time (flow of the simulation and fitting) are supposedly not possible. As an example, it is not possible to simulate the XRR scan without providing information about what MROX should simulate. Thus, the 'simulate' button is disabled until a layered structure is provided. Therefore, the hierarchy system is the system that governs the possible actions of the users towards MROX.

Layer operations system It consists of the sets of operations concerning the creation and manipulation of the layered structure shown in the table embedded in the MROX layout. There

are several actions available to the user: select the number of layers present in the heterostructure, divide a given layer by an integer number of layers, delete any layer, include a superlattice in-between any layer, etc. Furthermore, MROX provides a fast access list to the materials available in the database (DB). The fast access list and the DB are also editable. Therefore, the user may select the materials according to specific interests or research fields. The layer operation system is simple to use and makes MROX one of the easiest software for the simulation of XRR scans. Some of the default available materials are: 3C-SiC, AlAs, AlGaAs, AlP, AlSb, Au, cubic $CaMnO_3$, C-BN, C, CdS, CdSe, CdTe, Cu, Fe, Fe_3Si, GaAs, GaP, GaSb, Ge, HgS, HgSe, InAs, InSb, InP, La, $LaAlO_3$, MgO, Mo, $SrTiO_3$, W, ZnS, ZnSe, ZnTe and ZrO_2 for cubic lattices; 2H-SiC, 4H-SiC, 6H-SiC, AlN, AlGaN, AlInN, EuN, GaN, InN, InGaN, ZnO, hexagonal ZnS for hexagonal related lattices; MoO_3, $LaSrMnO_3$, orthorhombic $CaMnO_3$ for orthorhombic lattices. Although the above crystals are included in the software database (DB), user can easily introduce new crystals into the DB and provide shortcuts to MROX to include the new crystals as defaults.

Simulation system It consists in the required code to concretize the theoretical background exhaustively described in S1. The simulation is coded using two main developed functions: the 'simulate_callback' and the 'refractiveindex'. The latter is called within the former. The simulation may be performed with or without the experimental data. In the case of figure S2.2, the simulation of the XRR scan of sample E2 is shown. Sample E2 consists in a set of 3 Si/Ge periods grown on a Si buffer layer and 001 Si substrate. The final solution was presented in the main manuscript.
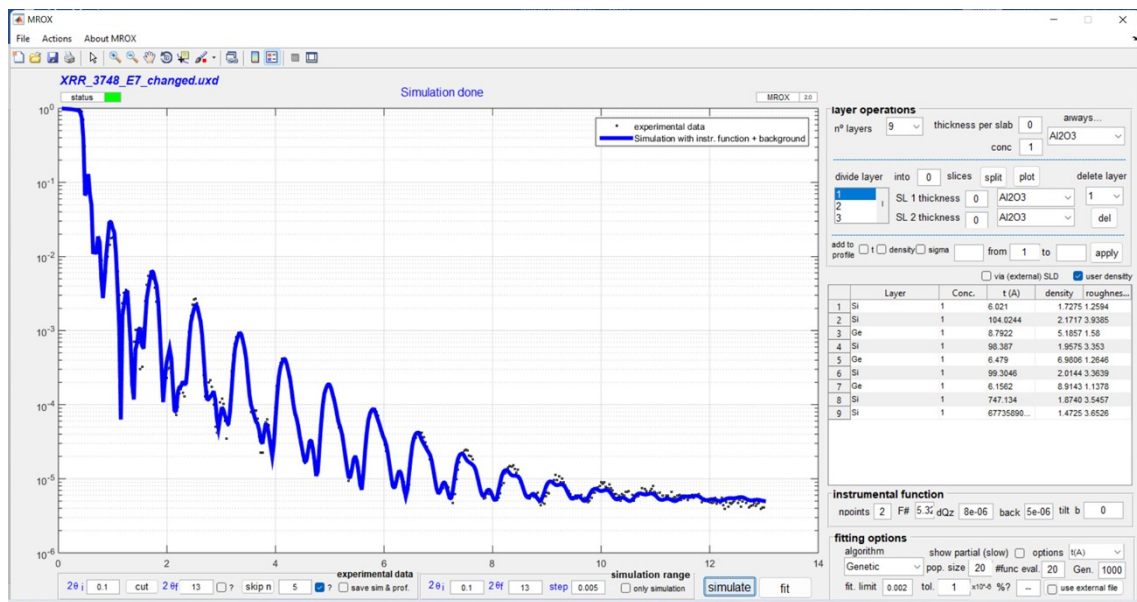

Figure S2.2 MROX layout (XRR version) highlights the experimental data of sample E2 together with the simulation.

The simulation incorporates the instrumental function. The software considers the instrumental function as the sum of a resolution function and a constant background. The resolution is determined by calculating the reflectivity averaged over several points, n, analytically defined by a Gaussian distribution and ranging from -a to a as:

$$R(Q_z) = \frac{\sum\limits_{a=-n}^{n} \omega_a R\left(Q_z\left[1 + \dfrac{a \delta Q_z}{n\, Q_z}\right]\right)}{\sum\limits_{a=-n}^{n} \omega_a}$$

Eq. S2.1

δQ_z is reciprocal space resolution and

$$\omega_a = exp\left(-2\left(\frac{a}{n}\right)^2\right)$$

Eq. S2.1

In the case of figure S2.2, the instrumental resolution is applied to two consecutive points (n_{points}=2) and an interval for Q_z of 8×10^{-6}. The linear background is 5×10^{-6}.

Fitting system The available fitting algorithms are the Genetic, the Pattern Search and the Simulated Annealing. There are two possible procedures to run the fit. The first consists in using an external file with the boundaries for each free variable. User may fit only the thickness of the individual layers, the density and the roughness and all the respective combinations, i.e., thickness and density, thickness and roughness, density and roughness and thickness, density and roughness to which the resolution functions is included. The second procedure is to change an input percentage to the specific free variables. In the second procedure, the resolution function is not included. The algorithms are supported by the available MATLAB Global Optimization and Optimization toolboxes but improved with new functionalities. Therefore, the only required toolbox is standard MATLAB. MROX software, complete instructions manual including several tutorials are available at MROX https://www.MROX.eu official website. The procedure to simulate and fit as well as the relevant theoretical background is also addressed in the instructions manual where a detailed description is presented. Moreover, complementary tutorials and new software releases with bug and error fixing and new functionalities are informed ot the MROX official webpage and Facebook page (www.facebook.com/MROXsoftware). Comments and suggestions are encouraged. Please send an email to smagalhes@ctn.tecnico.ulisboa.pt or use the social media platform for communication.

Saving system It consists in saving the outputs of a simulation or fitting by creating the files *datatable.dat* or datatable_fit.dat, respectively. The files have the following format depicted in table S2.1:

Table S2.1. Crystal designation (according to MROX DB), concentration (1 for binaries) thickness (in Å), mass density (in g/cm³) and roughness (in Å) of the 5 layers of sample E_1.

Crystal	Concentration	Thickness (Å)	Density (g/cm³)	Roughness (Å)
SiO_2	1	6.1	2.68	0.5
Si	1	95.4	2.4	2.09

Ge	1	9.5	5.36	4.95
Si	1	500	2.3	0.51
Si	1	----	2.33	0.51

Therefore, the output of a fit may be copied to the *datatable.dat* file a new simulation may be performed using as starting points the final solution found via the fit algorithm.

Figure S2.3 shows a flowchart with the procedure to simulate or fit a XRR scan. To run MROX, the user simply types MROX in the command window of the Matlab interpreter. After the validation of the license, two main routes are possible. The first consists in importing the experimental data. Here, several options are available for data manipulation. In fact, user may select a different range of the experimental data or even skip experimental datapoints which will reduce the computational effort and consequently, the time to simulate and/or to fit. The second option consists in designing the heterostructure under which the simulation is going to be executed.
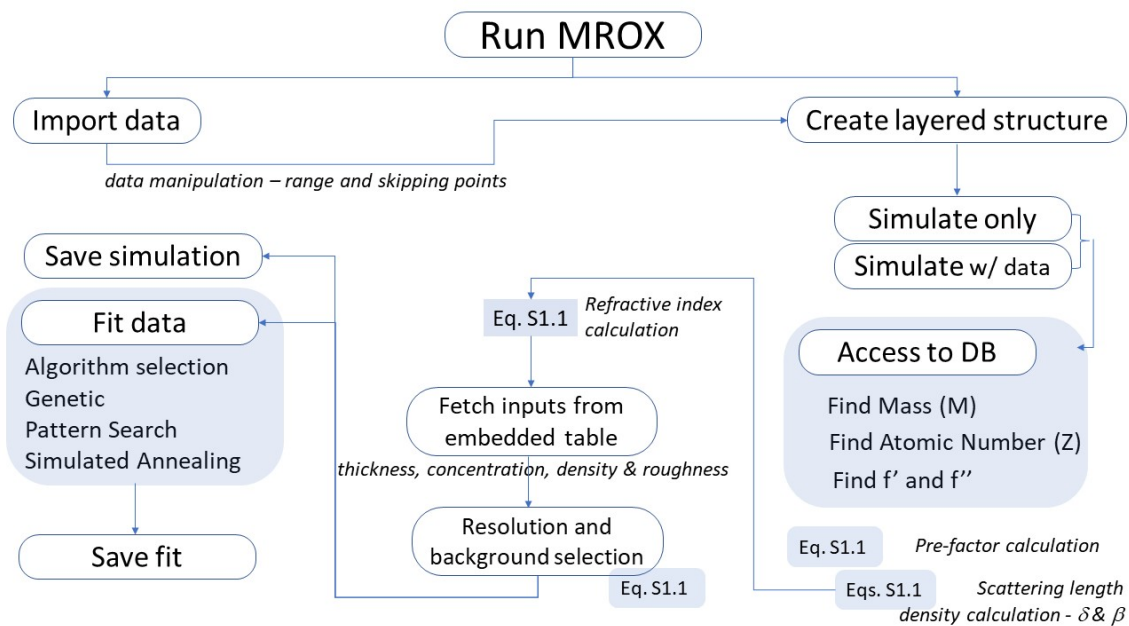

Figure S2.3 Flowchart showing the major steps in the simulation/fit of an experimental XRR scan or to simulate a layered structure.

The user may import the experimental data before or after creating a layered structure. After importing the data, the user may still only simulate the XRR scan of a layered structure by clicking on the ticking the 'simulate only' radio button (check figure S2.2). The function 'simulate' accesses the MROX DB and searches the elements present in the material in the database and then, fetches the atomic mass, atomic number (number of electrons) and f' and f'' to be used as

in the Eqs. S1.1-2. Then, it calculates the pre-factor ($\nu = \dfrac{Na\, r_e \lambda^2}{2\pi}$), the scattering length the refractive index of the materials of each layer. Next, MROX generates a matrix composed of the concentration, refractive index, scattering length density, thickness and roughness of each and starts the simulation function according to the described in section S.1. The instrumental function defined via a resolution function and a constant background according to Eq. S2.1 is employed in the calculations. The user may change the inputs in the layout embedded table and in instrumental function panel placed in the lower right panel of the graphical user interface. When any provisory solution is found via a trial-and-error approach, the user may click on the fitting button by choosing among the Genetic Algorithm, Pattern Search or Simulated Annealing. The three algorithms present advantages and disadvantages. The former is very useful when the initial solution is very far from the final solution. The drawback is that if the XRR scan presents several fringes, then the cost function that governs the goodness of the fit may pass the information to the algorithm engine that the fit converged but it is far from a good solution. On the other hand, the Pattern Search may solve this problem by increasing the time and the minimum number of iterations. Simulated annealing is very good to search close to the final solution.

References

[1] L. G. Parratt, *Surface Studies of Solids by Total Reflection of X-Rays*, Physical Review 95 (2): (1954) 359–369. doi:10.1103/physrev.95.359

[2] V. Holý, J. Kuběna, I. Ohlídal, K. Lischka, W. Plotz, *X-ray reflection from rough layered systems*, Phys. Rev. B 47 (23) (1993) 15896–15903.

[3] J. Als-Nielson, D. McMorrow, *Elements of Modern X-Ray Physics*, Wiley, New York (2001)

[4] J. Daillant, A. Gibaud, *X-Ray and Neutron Reflectivity: Principles and Applications*. Springer, (1999).

[5] M. Tolan, *X-Ray Scattering from Soft-Matter Thin Films*, Springer, (1999).

[6] P. Mikulík, *X-ray reflectivity from planar and structured multilayers*, Ph. D. thesis, University of Joseph Fourier, Grenoble, France (1997)

[7] H. Kiessig, *Untersuchungen zur Total reflexion von Röntgenstrahlen*, Annalen der Physik. Wiley. 402 (6): (1931) 715–768. doi:10.1002/andp.19314020607

[8] N. Nevot, P. Crocé, Rev. Phys. Appl. 15 (1980) 761. DOI:10.1051/rphysap:019800015030761900

[9] B. Vidal, P. Vincent, Appl. Optics 23 (1984) 1794-1801. DOI: 10.1364/AO.23.001794